



Impact energy and the risk of injury to motorcar occupants in the front-to-side vehicle collision

Leon Prochowski · Mateusz Ziubiński · Krzysztof Dziewiecki ·
Patryk Sz wajkowski

Received: 2 February 2022 / Accepted: 27 July 2022 / Published online: 28 August 2022
© The Author(s) 2022

Abstract The effects of a road accident where one vehicle hits its front on the side of another one are explored. In such cases, the impacted vehicle's side is usually significantly deformed, which causes a risk of serious injury to vehicle occupants. An analysis of the front-to-side collision covers many nonlinear and highly complex processes, especially when it is based on the collision energy balance. For the analysis, a model of a front-to-side motorcar collision and a dummy representing the impacted vehicle's driver

was prepared. The model simulations carried out were supplemented with important experimental test results. The model validation and the drawing of conclusions from research results were based on crash test results. The shares of major components in the front-to-side collision energy balance were determined. The impact energy has been proposed as an alternative predicate of the road accident effects; as a measure of the effects, the risk of injury to vehicle occupant's head and torso is considered. The model simulations were found to be in good conformity with experimental test results. The research results enabled determining the relation between the side impact energy and the risk of dummy's head and torso injuries according to the Abbreviated Injury Scale. The relation obtained was approximated using the logit model. This relation helps to reconstruct road accidents and to improve the car side's passive safety systems. A discussion of the results obtained has shown good consistence between the results of this work and other comparable research results.

L. Prochowski · M. Ziubiński (✉)
Institute of Vehicles and Transportation, Military
University of Technology (WAT), ul. gen. Sylwestra
Kaliskiego 2, 00-908 Warsaw, Poland
e-mail: mateusz.ziubinski@wat.edu.pl

L. Prochowski
e-mail: leon.prochowski@wat.edu.pl

L. Prochowski
Łukasiewicz Research Network—Automotive Industry
Institute (Łukasiewicz-PIMOT), ul. Jagiellońska 55,
03-301 Warsaw, Poland

K. Dziewiecki
University of Technology and Humanities in Radom, ul.
Malczewskiego 29, 26-600 Radom, Poland
e-mail: krzysztof.dziewiecki@uthrad.pl

P. Sz wajkowski
Electromobility Department, Łukasiewicz Research
Network—Automotive Industry Institute (Łukasiewicz-
PIMOT), ul. Jagiellońska 55, 03-301 Warsaw, Poland
e-mail: patryk.sz wajkowski@pimot.lukasiewicz.gov.pl

Keywords Front to side collision · Modelling of
motorcar collisions · Collision energy balance · Injury
risk · Abbreviated injury scale (AIS)

1 Introduction

In 2020, every third road accident in Poland was a front-to-side collision of moving vehicles [1], i.e. the incident where one vehicle hits the front of its body on the side of another one. In consequence of such a collision, a part of the kinetic energy of the impacting vehicle is transferred to the impacted one and changes its kinetic energy, body deformation work, etc. This part of the energy will be considered here as a measure of the side impact energy. Meanwhile, the risk of injury to vehicle occupants during the collision is a result of the dynamic effects exerted on the occupants taken together with the vehicle as well as of the forces and processes that take place in the zone of deformation of bodies of both vehicles. In this article, the risk of injury will be measured by the values of the indicators describing the dynamic loads on the head and torso of the occupants of the impacted vehicle.

In the case of a side impact, an important problem comes up, related to the deformation of the impacted vehicle's body, which results in an increase in the risk of injury, mainly to the near-side occupants [2, 3]. The research reported in [4] has shown that the average range of deformation of the impacted car's body part penetrating into the passenger compartment (car body deformation depth) is 0.37 m at the impact speed of 50 km/h and does not considerably depend on the car body size (or type). Such a deformation results in an occupant injury caused by structural components of the car body, such as the door or the B-pillar. A photo taken during a front-to-side crash test carried out by NHTSA [5] is presented in Fig. 1. It shows the car driver being struck by the deforming car body components.

There are many articles where the statistics of road accidents have been analysed from the point of view of the effects of motorcar collisions in various configurations. The analyses show low effectiveness of the

passive safety systems installed in the side part of vehicles. Additionally, it has been found in [6–8] that in the case of a significant deformation of the car body side, the actuation of the system of side airbags may cause an increase in the risk of injury to car occupants. This results in the fact that the injury risk in a car struck on its side is 2–8 times as high as the risk of a serious injury to an occupant of the frontally impacting car [9–11].

An analysis of the road accidents in the USA [13] within the scope of the vehicle occupant injuries that happened during front-to-side car collisions has shown that, in most cases, such injuries result from human body's contact with the vehicle door as well as with the B-pillar and steering wheel; the contact with the B-pillar causes the most serious injuries and the pillar deformation range has a considerable influence on the severity of the injuries. Therefore, when analysing the risk of injury arising during a front-to-side vehicle collision, it is important to take into account not only the inertial forces connected with the change in the vehicle's kinetic energy but also the nonlinear vehicle body deformation process. This indicates the particular need of analysing the processes of generating that risk and the possibilities of minimising it. An analysis of the design changes in the energy-absorbing zone in the vehicle side, introduced in order to limit the deformation caused by the collision, has been presented in [14]. Special attention has been paid, regarding this point of view, to improvements in the design of the driver's door [15–17] and the B-pillar [18–20]. In these publications, the possibility of applying reinforcing beams with various characteristics and special inserts aimed at partial absorption of the side impact energy has been analysed. The actions taken to improve the B-pillar included the selection of structural materials, pillar geometry, and integration of the pillar with the other components of the vehicle body. The results of those studies and research works



Fig. 1 Occupant struck by the side structure of the car body deforming when hit by the front of another car during a crash test; frames taken every 0.02 s from the beginning of the collision contact [12]

show that the actions taken within this scope are focused on increasing the energy absorption of these components, which is expected to bring a reduction in the penetration of the car body into the passenger compartment and thus to reduce the risk of injury to car occupants.

To estimate the injury risk, the AIS (Abbreviate Injury Scale) is often used [21]. In this scale, there are 6 degrees of severity of the injury to a human body (from 1-minor to 6-fatal). The risk of injury to the occupant of a car struck on its side, front, and rear, estimated according to the said scale, has been presented in [22]. The risk estimation results, obtained by computation, are shown in Fig. 2 as a function of the popularly used injury predicate Delta-V (defined as the difference between the pre-impact and post-impact vehicle speeds). The results have been determined for the AIS 4+ injuries, i.e. as a probability of severe injury to a human body. They confirm that for the same Delta-V value, the probability of suffering an injury during a front-to-side collision is much higher than that for other collision configurations. The use of Delta-V as a predicate of collision effects is not connected with the energy of such a collision, as the energy has a more general nature. However, Delta-V is now the most often used independent variable of such characteristic curves, despite the fact that its value is very difficult to be determined in the case of front-to-side collisions.

The issue of minimising the hazard to vehicle occupants constitutes now a large area for model tests, the results of which are often referred to the results of crash tests. The models used in such tests are of the spring-mass type (computational and dynamic), MBS (multi-body system) models, as well as FEM models (based on the finite element method) [23, 24]. In the mathematical descriptions of such models, the

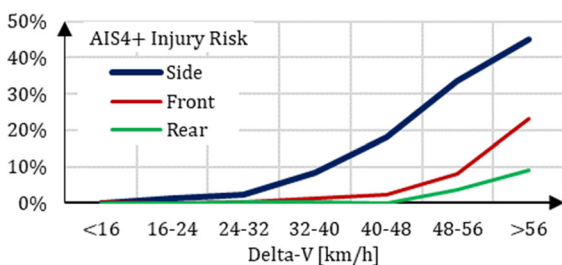


Fig. 2 The risk of an AIS 4+ injury to an occupant of a car struck on its side, front, and rear as a function of the impact speed (Delta-V) [22]

presence of nonlinear processes is taken into account, the processes usually being of the impact type and taking place during the vehicle collision, connected with such phenomena as friction in the tyre-road contact area, hysteresis and damping in the vehicle body deformation process, as well as vehicle movements in relation to each other [25]. The model tests are often carried out to represent the course of experimental tests, i.e. physical simulations of vehicle impacts against an obstacle or one vehicle being struck by another one or by a test carriage having the features of a real motor vehicle [26, 27].

The computation results presented in [28] have revealed the relation between the speed of a side impact of a vehicle against a concrete barrier and the risk of injury to vehicle occupant's torso. The computations were carried out using the flail-space model (FSM), where the human or test dummy is represented by a material point. The computation results were obtained in the form of a curve representing the risk of AIS 3+ and AIS 4+ injury to vehicle occupant's torso as a function of speed of the side impact of a vehicle against an obstacle. In this case, the impact speed may be a good reference measure because the problem was analysed for a vehicle impact against an undeformable concrete barrier instead of another deformable car.

An analysis of numerous articles with results of model tests on the front-to-side vehicle collision has shown that the use of models with up to 10 degrees of freedom [29] makes it already possible to study this issue with high conformity of the results obtained with experimental test results. For such models, the factor decisive for the obtaining of adequate conformity of the model with a real system is the selection of the nonlinear characteristics that describe the course of the impact processes taking place in the system in question. The use of the spacial model allows to conduct model tests with greater accuracy, but its result in significantly increase of amount of the data needed for modelling. Often, such data is difficult or impossible to measure in experimental research.

Interest is aroused by an analysis of the crash tests where a test carriage with a moving deformable barrier (MDB) [30] hits a side of the vehicle under consideration. The moving impacting block is a physical model of the vehicle front. The results of such tests predominate now when determining the probability of injury to vehicle occupants depending on Delta-V.

The method where the effects of road accidents are referred to Delta-V, predominating at present, derives from the previous analyses of frontal collisions. However, such a method of linking the causes with effects of road accidents is not fully applicable to the front-to-side collisions, especially when collisions between vehicles with different masses are considered. This problem has been signalled in [31]. Here, attention has been paid to the doubts about the using of Delta-V as the independent variable for the characteristic curves describing the collisions other than frontal. The authors have proposed the use of an indicator based on mechanical energy losses occurring during the collision. Such an approach has facilitated the interpretation of the results reported in [31], regardless of the direction and type of the vehicle collisions. The knowledge of the relations between the energy of a side collision and the injury risk is particularly useful in the road accident reconstruction process.

The issues described above constitute basic reasons for the research objective to be formulated as the identification of the relation between the energy of a side impact against a passenger car and the risk of injury to the occupants of the impacted vehicle. The exploration of this relation requires extending the knowledge of the course of the nonlinear processes that take place during the front-to-side collision and finds particular application to the issues related to the minimisation of injuries to vehicle occupants and the reconstruction of road accidents. The analysis will also cover determining the share of the energy of deformation of the side energy-absorbing zone in the side impact energy. The objective thus formulated will be pursued on the grounds of testing the nonlinear model of the dynamics of vehicle collision, integrated with the model of the test dummy. The test dummy model is used for determining the values of the biodynamic indicators, including the risk of injury to dummy's head and torso. Within the scope of this work, the front-to-side collision with an impact against the central area of the vehicle side will be analysed, because this is the configuration in which the biggest range of vehicle body deformation occurs [32]. During the tests, the observed risk of injury to vehicle occupants will be treated as a function of the energy of the side impact against the vehicle under consideration.

This article is an extension of the paper presented at the 16th International Conference “Dynamical Systems—Theory and Applications” DSTA 2021 [33].

2 Methods

The pursuance of the objective of this work will be based on model tests supplemented with results of experimental tests. The process of determining the relation between the vehicle's side impact energy and the risk of injury to occupant's head and torso is illustrated in Fig. 3.

The energy balance of a front-to-side vehicle collision has the form:

$$E_{KA} + E_{KB} = E_{KA}^* + E_{KB}^* + W_{DAB} + W_{TAB} + W_{FAB} + E_R, \quad (1)$$

where,

E_{KA}, E_{KB} —kinetic energy of the impacting vehicle (A) and the vehicle struck on its side (B) at the instant of the beginning of the contact phase of vehicle collision (in case of front-to-side collision sum of these energies is treated as impact energy);

E_{KA}^*, E_{KB}^* —kinetic energy as above, but at the end of the vehicle collision process;

$W_{DAB} = W_{DA} + W_{DB}$ —work of deformation of the bodies of vehicles A and B;

W_{TAB} —work of the friction forces in the zone of contact between the vehicle bodies;

$W_{FAB} = W_{FA} + W_{FB}$ —work of the forces of resistance to motion of vehicles A and B; in the front-to-side vehicle collision, $W_{FB} \gg W_{FA}$;

E_R —the remaining energy part, related to other processes that take place during the vehicle collision.

In result of the front-to-side vehicle collision, the initial energy ($E_{KA} + E_{KB}$) is divided into the energy received by vehicle A ($E_{KA}^* + W_{DA}$), energy received by vehicle B ($E_{KB}^* + W_{DB}$), and dissipated energy ($W_{TAB} + W_{FAB} + E_R$). The energy received by vehicle B by the end of the compression phase of the collision process, i.e. the phase, during which the deformation is increasing and the risk of injury to vehicle occupants is emerging, will be referred to as the side impact energy E_{SI} . Thus, we have:

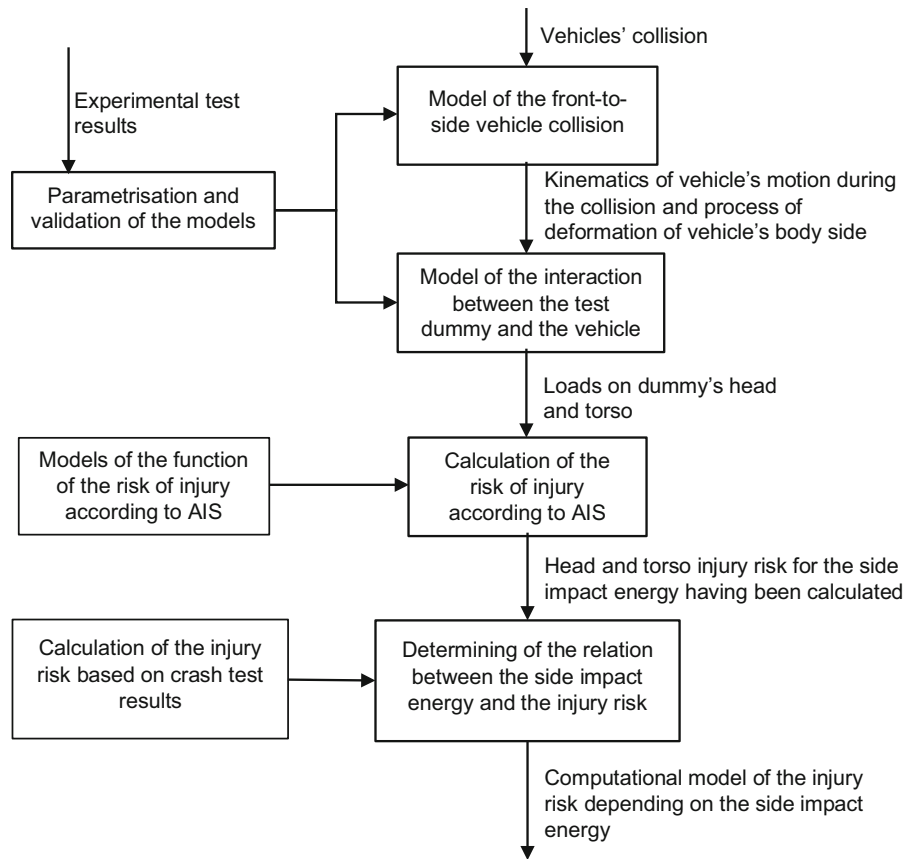


Fig. 3 Schematic diagram of the information transformation process to pursue the work objective

$$E_{SI} = E_{KB}^*(t = t_{END}) + W_{DB}(t = t_{END}) - E_{KB}(t = 0), \quad (2)$$

where: t_{END} —time of the end of the compression phase of the collision process.

An important good point of such an approach to the energy balance of a vehicle collision is not only the fact that it covers many components of the balance but also sensitivity of the balance to results of the works reported previously and concerning the raising of the energy absorption of the vehicle body side. This is provided for in the component W_{DAB} . Some of the components (terms) included in (1) can be precisely estimated from the accident effects observed (vehicle body deformation and vehicle position). However, problems arise from the fact that the above factors depend on the largely nonlinear processes that take place during the collision. Such processes were analysed by the authors in [34, 35]. Figure 4 shows dependences of the vehicle impact forces on the

combined deformation of the vehicle bodies in the front-to-side crash test. The dependences were determined from the available results of experimental tests carried out by NHTSA (USA) [12]; those results were also used for the computing of the deformation work W_{DAB} . Figure 5 shows the force of resistance course during the lateral direction movement, when the vehicle struck on its side is slid with increasing lateral slip ratio s_y . These characteristics result in nonlinear nature of changes in energy E_{FB} as a function of the sideward vehicle displacement.

2.1 Model of the front-to-side vehicles' collision

A model of the front-to-side vehicle collision was prepared in the MATLAB programme. The model is shown in Fig. 6. It has been preliminarily presented by the authors in [39]. For the k th vehicle ($k = [A, B]$), the following external interactions are taken into account:

Fig. 4 Impact force vs combined deformation of vehicle bodies in the front-to-side crash test; Honda Accord car side impact with the velocity of 48 km/h (source: own calculations presented in [35])

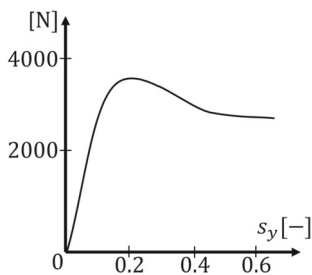
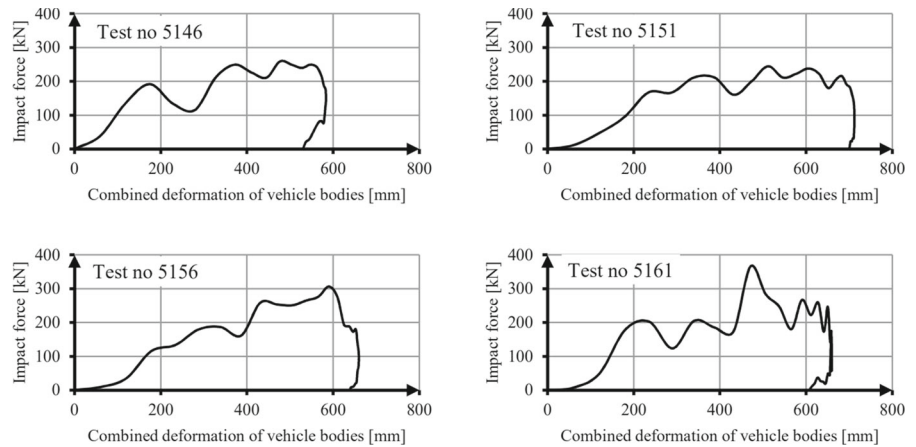


Fig. 5 Example of the force of resistance to lateral tyre sliding vs the tyre slip ratio [25, 37, 38]

- Tangent road reaction forces T_{ki} (e.g. T_{B1}), acting on the car body via the wheel suspension system and applied in the area of contact of the i th tyre with the road at points of support (denoted as 1, 2, 3, 4); these reaction forces are determined by using the TMeasy tyre-road interaction model [37, 40];
- Resultant force $F_k(F_A, F_B)$ of contact between the crashing vehicles, applied at point $E_k(E_A, E_B)$ at the boundary of the areas of deformation (drawn as heavy line).

The geometry of the vehicle solids, positions of the points of support in the centres of the tire-road contact areas 1, 2, 3, 4, as well as positions of the centre of gravity $C_k(C_A, C_B)$ and of the vehicle contact force $E_k(E_A, E_B)$ have been defined in the local coordinate system $O_k u_k v_k$ attached to the car body solid (Fig. 6). The coordinates of points E_A and E_B are identical to each other in the global coordinate system OXY .

The k th vehicle positions are defined by matrix of generalised coordinates in the form:

$$q_k = [x_{ok}, y_{ok}, \psi_k]^T, \tag{3}$$

where x_{ok}, y_{ok} —coordinates of the origin of the local coordinate system of k th vehicle in the global system; ψ_k —angular vehicle position; $k = [A, B]$.

The kinematics of the centres of mass C_A, C_B has been described as follows:

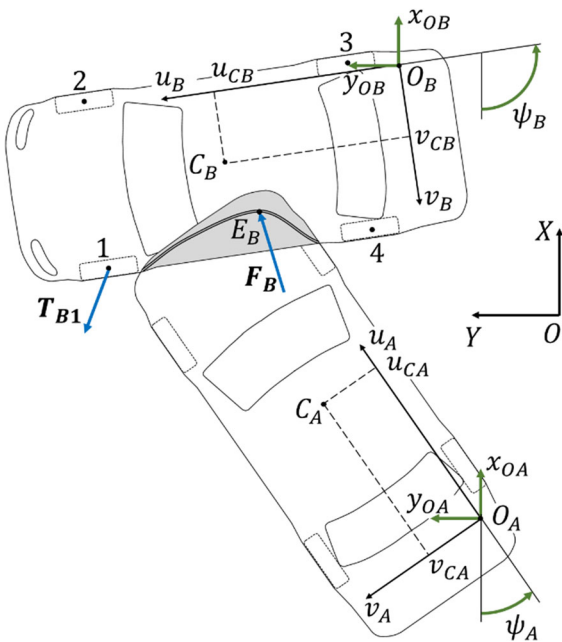


Fig. 6 Model of the vehicle collision

$$\begin{aligned} \begin{bmatrix} x_{Ck} \\ y_{Ck} \end{bmatrix} &= \begin{bmatrix} x_{Ok} \\ y_{Ok} \end{bmatrix} + \Phi_k \begin{bmatrix} u_{Ck} \\ v_{Ck} \end{bmatrix} \\ \begin{bmatrix} \dot{x}_{Ck} \\ \dot{y}_{Ck} \end{bmatrix} &= \begin{bmatrix} \dot{x}_{Ok} \\ \dot{y}_{Ok} \end{bmatrix} + \dot{\psi}_k \tilde{\Phi}_k \begin{bmatrix} u_{Ck} \\ v_{Ck} \end{bmatrix} \\ \begin{bmatrix} \ddot{x}_{Ck} \\ \ddot{y}_{Ck} \end{bmatrix} &= \begin{bmatrix} \ddot{x}_{Ok} \\ \ddot{y}_{Ok} \end{bmatrix} + \left(\ddot{\psi}_k \tilde{\Phi}_k - \dot{\psi}_k^2 \Phi_k \right) \begin{bmatrix} u_{Ck} \\ v_{Ck} \end{bmatrix} \end{aligned} \tag{4}$$

$$\begin{aligned} \Phi_k &= \begin{bmatrix} \cos(\psi_k) & -\sin(\psi_k) \\ \sin(\psi_k) & \cos(\psi_k) \end{bmatrix}; \tilde{\Phi}_k \\ &= \begin{bmatrix} -\sin(\psi_k) & -\cos(\psi_k) \\ \cos(\psi_k) & -\sin(\psi_k) \end{bmatrix}. \end{aligned} \tag{5}$$

The vehicle motion has been described by the following equations in the global system *OXY*:

$$\begin{aligned} m_k \ddot{x}_{Ck} &= \sum_{i=1}^4 T_{kix} + F_{kx} \\ m_k \ddot{y}_{Ck} &= \sum_{i=1}^4 T_{kiy} + F_{ky} \\ J_{Ck} \ddot{\psi}_k &= \sum_{i=1}^4 M_{CTki} + M_{CFk}, \end{aligned} \tag{6}$$

where m_k, J_{Ck} —mass and mass moment of inertia of the k th vehicle;

M_{CTki}, M_{CFk} —moments of forces $T_{ki}(T_{kix}, T_{kiy})$ and $F_k(F_{kx}, F_{ky})$ relative to the centre of mass of vehicle C_k .

In consideration of the typical construction of cars with sedan-type bodies and of the experimental test results [12] related to the identification of their properties concerning the energy dissipation during a collision, the car body solid in the deformation area was hypothetically divided into zones with different elastoplastic properties. The idea of the division is

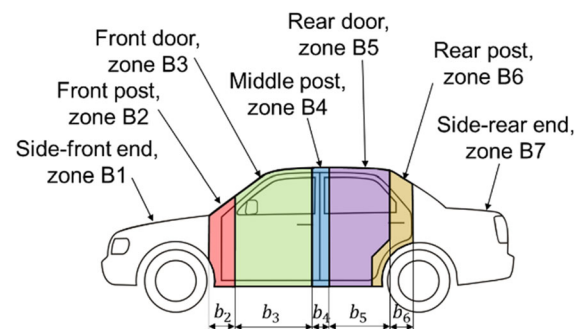


Fig. 7 Division of the body of vehicle B into zones with different elastoplastic characteristics

presented in Figs. 7 and 8. In the side of vehicle B, seven zones with different properties were distinguished. Similarly, the front part of vehicle A was divided into five zones, which constitute a system of zones with symmetric characteristics on the left and right vehicle side.

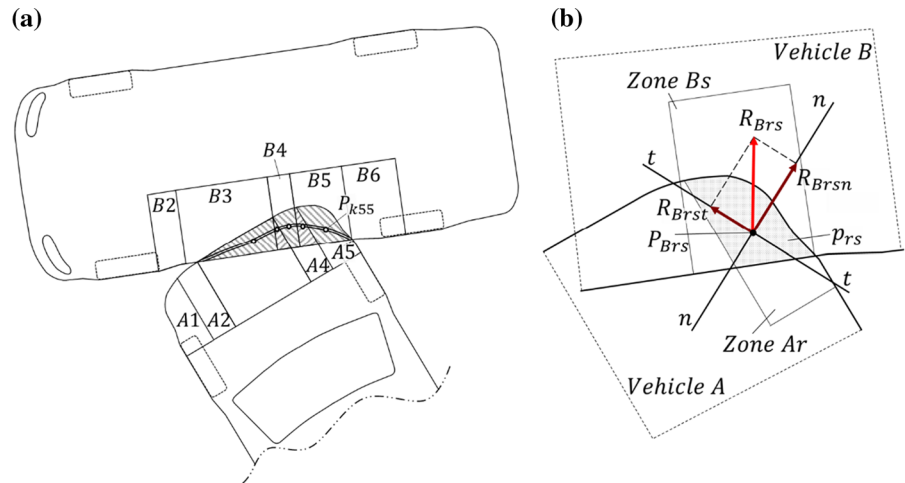
An important stage of developing the vehicle collision model is the preparation of a procedure to determine the contact force F_k between the vehicle bodies. Many various methods and models used to calculate the contact forces can be found in the literature [41, 42]. In the case of a motorcar collision, the nonlinear characteristics of the cars involved that are important for the car body deformation process must be taken into account. The problem of nonlinearity of the phenomena that take place during the collision of solids has been analysed in [43]. That publication provides a review of the computational and empirical models intended for the calculation of contact forces, where one of the independent variables in the function describing the forces is the area of interpenetration of the solids being in contact. Based on an analysis of the area of interpenetration of the solids, a procedure was developed to calculate F_k .

At every calculation step of the vehicles' motion simulation, based on the kinematics results, among others, the relative position and orientation of the motorcars on the road, and the linear and angular velocities of the vehicles are determined. The collision between vehicle A and vehicle B is identified on the basis of the penetration area of the bodyworks outlines. In the area of this penetration, we have the above-mentioned zones. The zones interpenetration is shown in Fig. 8.

An example of the vehicles positions during their collision is shown in Fig. 8a. The area of interpenetration of the bodyworks has been hatched, in which the zones from the vehicles A and B are marked.

The resultant force F_k of contact between the crashing vehicles and the point E_k of application of this force (Fig. 6) results from force vectors R_{krs} summing. The elementary contact forces R_{krs} (Fig. 8b) are generated by the pairs of contacting zones (where r and s are indices of individual zones in cars A and B, respectively, i.e. A_r is a zone in the body of car A and B_s is a zone in the body of car B). Each of these forces reflects the size of deformation in the specific zone. The following was assumed for

Fig. 8 Schematic diagram for determining the forces of contact between the crashing vehicles: **a** zones in the bodies of cars A and B; **b** force R_{Brs} exerted on the body of car B in result of the contact of the zones Ar and Bs; point P_{k55} in Fig. 8a corresponds to P_{Brs} in Fig. 8b



calculating the elementary contact forces R_{krs} between two zones (Fig. 8b):

1. The zones are convex figures.
2. The tangent direction $t-t$ of the interaction between the zones is parallel to the straight line going through the points of intersection of the edges of zones Ar and Bs. The normal direction $n-n$ is perpendicular to $t-t$.
3. The position of points P_{krs} (Fig. 8a, b) is defined by the size of the area p_{rs} of contact between the zones. Its situated on the boundary of the areas of deformation (drawn as heavy line in Fig. 6) between the vehicle body deformation areas p_{Ar} and p_{Bs} (where $p_{Ar} + p_{Bs} = p_{rs}$). The shares of areas p_{Ar} and p_{Bs} are determined on the grounds of the elastoplastic and damping characteristics of zones Ar and Bs. At every instant, we have points P_{Ars} (attached to the body of car A) and P_{Brs} attached to the body of car B and having the same coordinates in the global coordinate system OXY . At these points, the contact force R_{krs} is applied, whose value is determined by the deformation range and the course of the nonlinear curve characterising the deformation in the zone.
4. The normal component R_{krsn} of the contact force R_{krs} is always a force repulsing the vehicles from each other (Fig. 8b); depends on the area p_{rs} of contact between the zones and on the deformation velocity $v_{A/B}$:

$$R_{krsn} = R_{krsn}(p_{rs}) + R_{krsn}(v_{A/B}), \tag{7}$$

where the deformation velocity $v_{A/B}$ in the zone, i.e. the velocity of point P_{Ars} in relation to point P_{Brs} , is calculated as follows:

$$v_{A/B} = v_{PArs} - v_{PBrs}. \tag{8}$$

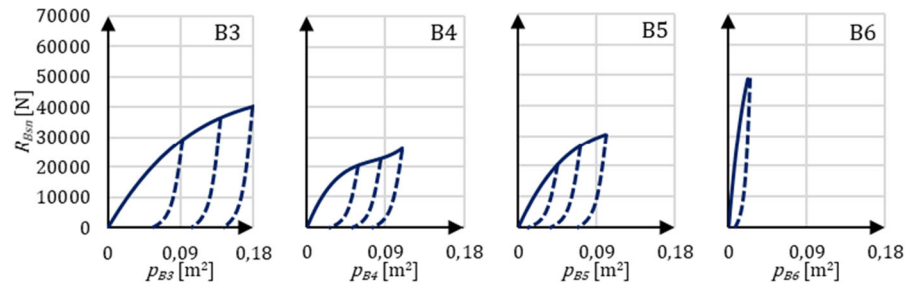
5. The tangent component of the contact force R_{krs} is calculated from the equation:

$$R_{krsst} = \mu_{rs} R_{krsn}, \tag{9}$$

and is always so directed that it impedes the motion of the car body zones in relation to each other. As μ_{rs} the coefficient of kinetic friction in the contact area between the zones has been marked. Based on the analysis of the front-to-side vehicles' collision in experimental tests, a value of μ_{rs} was adopted as constant 0.2.

In Fig. 8a, as an example, there are five zone pairs, the number and combination of which depend on instantaneous car body positions relative to each other. When the collision model is calculated, the common interpenetration area value p_{rs} is determined at every time step for each pair of the zones and the value of the contact force between the zones is determined based on this. The characteristic curves $R_{Arn}(p_{Ar})$ and $R_{Bsn}(p_{Bs})$ have been determined and presented by the authors in [39]. The curves plotted for zones B3–B6 on a sedan-type car body side have been shown as an example in Fig. 9. Based on $R_{Arn}(p_{Ar})$ and $R_{Bsn}(p_{Bs})$ characteristics, the curve of $R_{rsn}(p_{rs})$ is prepared and use in Eq. (7). Moreover, in the calculation example considered in this study an assumption was adopted that $R_{krsn}(v_{A/B}) = 0$.

Fig. 9 Curves describing the nonlinear dissipation properties of individual zones on a car body side (source: own calculations presented in [39])



According to the number of pairs of interacting zones, we have the same number of elementary contact forces \mathbf{R}_{krs} . They form a system of forces and on their basis the resultant force \mathbf{F}_{k} , is determined, and its components appear in the equations of motion (6) as $F_{\text{kx}}, F_{\text{kly}}, M_{\text{CFk}}$. The point of its application E_{k} is always on the boundary of the areas of deformation (heavy line in Fig. 6) and replaces the points P_{krs} (Fig. 8) which define this boundary of deformation areas.

The procedure for determining the resultant contact force \mathbf{F}_{k} at every step of the front-to-side vehicles' collision calculation is as follows:

1. Determining the relative position of vehicles A and B (based on the results of calculations of their kinematics in the previous step of calculations).
2. Identification of pairs of Ar–Bs zones with common p_{rs} areas.
3. Calculation of p_{rs} values for all pairs of Ar–Bs zones.
4. Calculation of elementary contact force components R_{krsn} and R_{krst} in pairs of Ar–Bs zones, according to (7) and (9).
5. Determination of the values of p_{Ar} and p_{Bs} , based on the value of R_{krsn} and the data for modelling (Fig. 9).
6. Determination of the position of the points P_{krs} in the $O_{\text{k}}u_{\text{k}}v_{\text{k}}$ coordinate systems (based on the values of p_{Ar} and p_{Bs}) and the orientation of the P_{krsnt} coordinate systems (Fig. 8b).
7. Calculation of the resultant contact force \mathbf{F}_{k} from the system of \mathbf{R}_{krs} forces.
8. Determination of the position of the point E_{k} in the coordinate system $O_{\text{k}}u_{\text{k}}v_{\text{k}}$ on the basis of the set of P_{krs} points.
9. Solution of the system of equations of the vehicle motion (6) (based on results of the calculations from points 7 and 8 of the procedure) and the

kinematics of the vehicles determination for the next step of front-to-side collision calculation.

The curve characterising the deformation in the compression phase were approximated by polynomial as follows:

$$R_{\text{Bsn}}(p_{\text{Bs}}) = k_1 p_{\text{Bs}}^3 + k_2 p_{\text{Bs}}^2 + k_3 p_{\text{Bs}} \quad (10)$$

where k_1, k_2, k_3 —coefficients of the approximating polynomial, obtained by the least squares method. Values of these coefficients for different characteristics of vehicle's body zones has been collected in Table 1.

The results of the front-to-side vehicles' collision model calculations are used to investigate the vehicle's interaction with the test dummy (Fig. 3).

2.2 Test dummy and vehicle interaction model

The modelling process at this stage is aimed at representing the interaction between the test dummy and the car body side, observed during experimental (crash) tests (Fig. 1). During the crash tests, the test dummies play the role of measuring instruments. Those used in the front-to-side vehicle crash tests often include the ES-2re dummies (e.g. in the tests carried out to the FMVSS 214 or NHTSA procedures [5]) and the SID-IIIFRG dummies (e.g. in the tests carried out to the procedures adopted by NCAP and EURO-NCAP [44]). In the front-to-side collision model, the ES-2re dummy was used to represent the vehicle driver/occupant seated in vehicle B. Such a dummy makes it possible to determine the kinematic and dynamic processes in order to calculate the biodynamic indicators of head and torso injuries.

In the analysis, an assumption was made that the presence of a dummy in the car has a negligible impact on the vehicles' motion during the collision and on the process of deformation of vehicle bodies. On the other

Table 1 Polynomial coefficients values

	k_1	k_2	k_3
Zone B3	3.2538E + 06	- 2.3020E + 06	+ 6.1130E + 05
Zone B4	5.0128E + 07	- 1.1312E + 07	+ 9.5822E + 05
Zone B5	2.7995E + 07	- 1.0583E + 07	+ 1.5016E + 06
Zone B6	6.1754E + 08	- 8.7026E + 07	+ 4.6033E + 06

hand, the vehicle motion causes the dummy to move. The dummy’s position in vehicle B at the instant $t = 0$ has been presented in Fig. 10. The following notation has been adopted:

- M_D —mass of the dummy;
- u_D, v_D —coordinates of dummy’s position in the $O_B u_B v_B$ system;
- Δv —clearance between the dummy solid and the vehicle body side at the instant $t = 0$;
- w_D —dimension of dummy’s head or torso;
- $v_{Bc}(t)$ —coordinate describing the penetration of the car body side into the passenger compartment and the deformation of the car body side in the area of contact with the dummy solid at the instant t ; at $t = 0$, we have $v_{Bc}(t = 0) = v_{BD}(t = 0) + w_D + \Delta v$;
- $k_{uB1}, k_{vB1}, d_{uB1}, d_{vB1}$ —characteristics describing the spring-damping interaction between the dummy and the car seat;
- k_{vB2}, d_{vB2} —characteristics describing the spring-damping interaction between the dummy and the car body side being deformed.

The issue under analysis is the dummy’s motion in the local coordinate system $O_B u_B v_B$ attached to the vehicle. In the analysis, the authors take into consideration the interactions between the dummy and its seat (moving together with the coordinate system

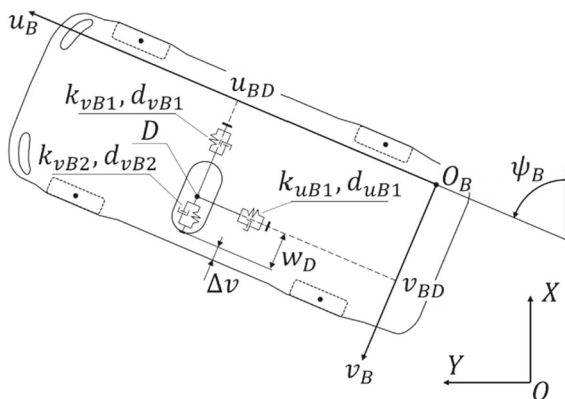


Fig. 10 Position of dummy D for $t = 0$

$O_B u_B v_B$) and between the dummy and the car body side at the values of the Δv clearance (distance between the dummy side and the vehicle body) varying in result of deformation w_B . The modelling covers the interaction between dummy’s head and torso (D in Fig. 10) and the vehicle structure. The said interactions cause deformations in the spring-damping components linking the D solid with the seat and car body side. A similar pattern of the interaction between the dummy and its surroundings has been adopted in [45, 46].

In result of a front-to-side vehicle collision, a side of the impacted car is deformed. The deformation depth in the area where the dummy solid may be present within time t is described by coordinate $v_{Bc}(t)$. The coordinate is determined from the positions of points $P_{Brs}(t)$ (Fig. 8b) taken during the collision process. After the clearance Δv has been used up, the dummy solid begins to interact with the car body side being deformed. An example of the system configuration for the time instant $t \neq 0$ is presented in Fig. 11.

The interaction between the dummy and its seat and car body side translate into forces f_D and their components f_{vB1}, f_{vB2} , and f_{uB1} marked in Fig. 11. Their values at the instant t are calculated as follows:

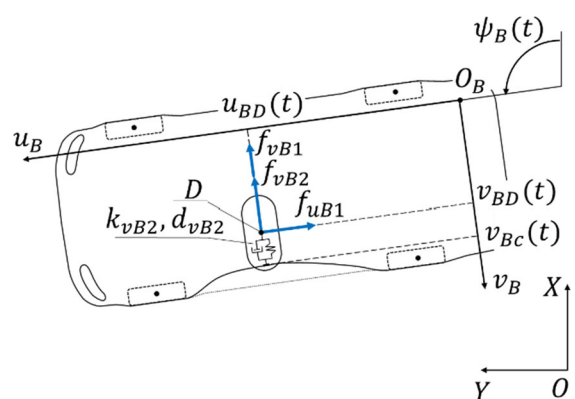


Fig. 11 Position of dummy D at the time instant $t \neq 0$

$$f_{uB1}(t) = k_{uB1}[u_{BD}(t) - u_{BD}(t=0)] + d_{uB1}\dot{u}_{BD}(t) \quad (11)$$

$$-f_{vB1}(t) = k_{vB1}[v_{BD}(t) - v_{BD}(t=0)] + d_{vB1}\dot{v}_{BD}(t) \quad (12)$$

$$f_{vB2}(t) = \begin{cases} 0 & \text{if } v_{Bc}(t) - w_D - v_{BD}(t) \geq 0 \\ k_{vB2}[v_{Bc}(t) - v_{BD}(t) + w_D] + d_{vB2}[\dot{v}_{Bc}(t) - \dot{v}_{BD}(t)] & \text{if } v_{Bc}(t) - w_D - v_{BD}(t) < 0 \end{cases} \quad (13)$$

The differential equations of dummy's dynamics have the form:

$$M_D \begin{bmatrix} \ddot{x}_D \\ \ddot{y}_D \end{bmatrix} = \begin{bmatrix} F_{Dx} \\ F_{Dy} \end{bmatrix}. \quad (14)$$

The vector of force f_D acting on the dummy has the following form in the local system $O_B u_B v_B$:

$$f_D = \begin{bmatrix} f_{uB1} \\ f_{vB1} + f_{vB2} \end{bmatrix}. \quad (15)$$

In the global coordinate system, it takes the form:

$$F_D = \begin{bmatrix} F_{Dx} \\ F_{Dy} \end{bmatrix} = \Phi_B f_D. \quad (16)$$

The kinematics of the dummy solid in the global coordinate system OXY is determined as follows:

$$\begin{bmatrix} x_D \\ y_D \end{bmatrix} = \begin{bmatrix} x_{OB} \\ y_{OB} \end{bmatrix} + \Phi_B \begin{bmatrix} u_{BD} \\ v_{BD} \end{bmatrix} \quad (17)$$

$$\begin{bmatrix} \dot{x}_D \\ \dot{y}_D \end{bmatrix} = \begin{bmatrix} \dot{x}_{OB} \\ \dot{y}_{OB} \end{bmatrix} + \dot{\psi}_B \tilde{\Phi}_B \begin{bmatrix} u_{BD} \\ v_{BD} \end{bmatrix}$$

$$\begin{bmatrix} \ddot{x}_D \\ \ddot{y}_D \end{bmatrix} = \begin{bmatrix} \ddot{x}_{OB} \\ \ddot{y}_{OB} \end{bmatrix} + \left(\ddot{\psi}_B \tilde{\Phi}_B - \dot{\psi}_B^2 \Phi_B \right) \begin{bmatrix} u_{BD} \\ v_{BD} \end{bmatrix}.$$

In (16) and (17), Φ_B and $\tilde{\Phi}_B$ are calculated according to (5).

The above equations define the kinematic and dynamic interactions between vehicle B and the dummy. Based on results of these calculations, the injury risk arising during a road accident is forecasted (Fig. 3). The injury risk is expressed by means of biomechanical injury criteria. For the ES-2re dummy intended for the front-to-side crash tests, the following injury criteria are distinguished among other ones [47]:

- Head Injury Criterion (HIC) calculated from the equation:

$$\text{HIC36} = \max \left[\frac{1}{t_2 - t_1} \int_{t_1}^{t_2} a(t) dt \right]^{2.5} (t_2 - t_1), \quad (18)$$

where $a(t)$ is the resultant head acceleration in a time interval from t_1 to t_2 , $t_2 - t_1 \leq 0.036$ s, and this time interval is the one when the highest acceleration values occur;

- Thoracic Injury Criteria, estimated from the results of calculation of deflection of ribs or torso.

The following functions were used for the forecasting of the injury risk:

$$a(t) = \sqrt{\dot{x}_D^2 + \dot{y}_D^2} \quad (19)$$

$$\begin{aligned} \text{mrrib} &\rightarrow \max \text{ rib deflection} \\ &= \max[v_{BD}(t) - v_{Bc}(t) + w_D]. \end{aligned} \quad (20)$$

The values of the biomechanical injury criteria provide a basis for the calculations of the risk of injury to the human body according to the Abbreviated Injury Scale (AIS) [21]. Based on [47], the probability of injury to the ES-2re dummy was calculated:

$$P(\text{AIS } 3+) = N \left(\frac{\ln(\text{HIC36}) - 7.45231}{0.73998} \right) \quad (21)$$

$$P(\text{AIS } 3+) = \frac{1}{1 + e^{(2.0975 - 0.0482 \cdot \text{mrrib})}}, \quad (22)$$

where the formula (21) is used to calculate the probability of head injury based on the normal distribution function N , the argument of which is the HIC36 value, and the formula (22) is used to calculate the injury probability based on the value of the maximum deflection of dummy's ribs or torso.

2.3 Validation and parametrisation of the model

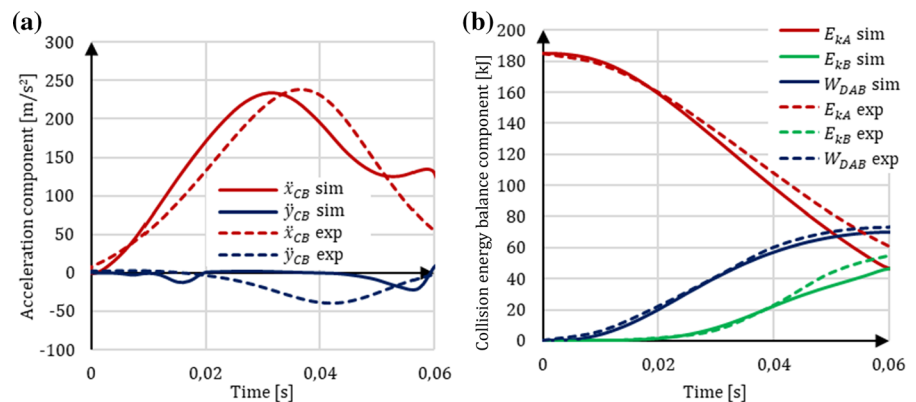
The procedure of validation of the front-to-side vehicle collision model has been presented by the authors in [39]. The parametrisation and validation of the model was based on results of front-to-side vehicle crash tests (Fig. 3). For this purpose, results of experimental tests carried out at the Łukasiewicz Research Network—Automotive Industry Institute (Ł-PIMOT) were used. These test results have been presented, inter alia, in [34]. For the tests, Honda

Accord cars manufactured in 2000–2002 were used. The experiment results used for the analysis were obtained from front-to-side vehicle crash tests, where the impacted car moved with a constant speed or was standing still, depending on the model validation needs. The model parameters were categorised as those measurable (e.g. mass and inertia data, geometrical dimensions), computable (e.g. elastoplastic characteristics of the front car body part, forces of the resistance to motion), and having to be estimated (i.e. the data that describe the elastoplastic and damping characteristics of individual zones in the car body side). In the model validation process, attention was focused on the parametrisation of the data of the third category. Initial values of the parameters sought were assumed based on the analysis of the results of experimental tests. The simulation calculations of the front-to-side vehicles' collision for the initial values of the parameters were prepared and performed. The obtained results were compared with the results of experimental tests as a part of event validity. The compliance of some physical quantities describing the kinematics of a vehicle's lateral impact was assessed using the operational graphics method. The linear correlation coefficient was chosen as the criterion for assessing compliance.

The following experimental test and simulation results have been summarised in graphical form in Figs. 12 and 13, as a results of an experimental verification of the model:

- Time histories of car B acceleration;
- Course of the car body side deformation during the vehicle collision;
- Energy balance components for the compression phase.

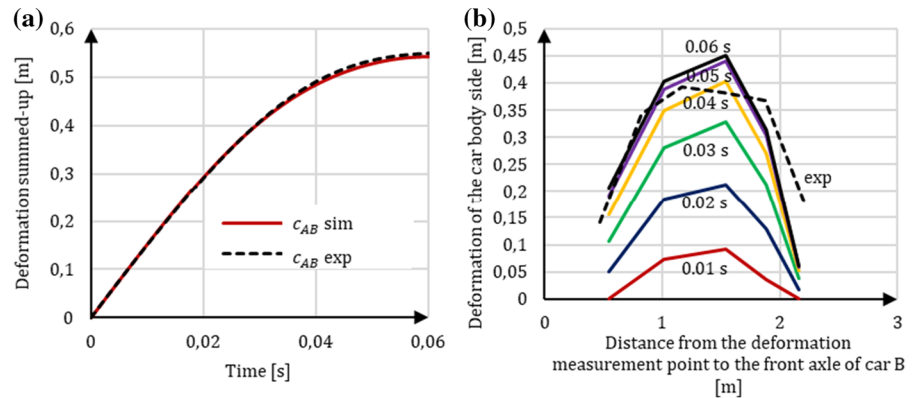
Fig. 12 Summary of changes in the components of the centre of mass acceleration vector (a) and changes in the values of the collision energy balance components during the compression phase (b)



In Fig. 12, the dashed lines represent the results of experimental tests and the solid lines represent the results of simulation computations. Good conformity can be seen between the curves representing changes in the components of the acceleration vector of the vehicle B centre of mass, obtained experimentally and by simulations (Fig. 12a). The red colour indicates the curves plotted for the acceleration component in the impact direction, i.e. in the direction of generating the dynamic deformation of the vehicle body. Figure 12b presents the time history of changes in the values of several individual components of the collision energy balance during the compression phase. The graph shows changes in the kinetic energy of car A (E_{KA} , red), kinetic energy of car B (E_{KB} , blue), and sums of the work of deformation of the bodies of cars A and B (W_{DAB} , green). The results obtained show good conformity between the energy-related processes in model simulations and experimental tests.

The deformation growth process is presented in Fig. 13. Figure 13a shows the course of growth in the dynamic deformation, identified as the change in the distance between the centres of mass of the vehicles during the contact phase of their collision. This means that the curve represents the summed-up deformation of both the vehicles involved. Figure 13b, in turn, shows changes in the contour of deformation of the vehicle body side during the contact phase of the collision; $t = 0.06$ s corresponds to the end of the phase of compression of the vehicle bodies (t_{END}). This identifies the deformation development process at several points on the vehicle side. The dashed line shows the contour of the permanent deformation, measurable after the crash test. The maximum range of the dynamic deformation, determined by the

Fig. 13 Vehicle A and B body deformation growth process (a) and characteristic values of the deformation of the vehicle body side (b)



numerical calculations for the instant $t = 0.06$ s, is connected with the fact that the deformation also includes the elastic deformations, which cannot be measured after the end of the collision process.

The dummy-vehicle interaction model was validated separately. Within this scope, results of the NHTSA experimental tests [12] were used for the parametrisation and validation of the car collision model. The experiments taken as a reference were the front-to-side motorcar crash tests Nos. 5146, 5151, 5156, 5161 [12], where the side impact energy amounted to 110–150 kJ and the Honda Accord car was the impacted vehicle, like in [34]. In the impacted vehicle, an ES-2re test dummy was placed on driver's seat and the values of the parameters enabling the forecasting of the probability of injury were recorded by means of sensors installed in the dummy.

During the parametrisation and validation of the model of the dummy placed on driver's seat, calculations were carried out for the simulation of a front-to-side collision, where the side impact energy and the initial conditions identical to those of the experimental tests were represented. The model parameter values have been gathered in Table 2. The characteristics of the spring-damping interactions between the dummy and the car seat and between the dummy and the car body side are progressive; they also depend on the range and speed of such interactions. The data specified in Table 2 are averaged parameter values corresponding to the initial, approximately linear, fragment of the characteristic curves.

Example results of the validation of the ES-2Re dummy model are presented in Fig. 14. Figure 14a shows the time function of rib deflection resulting from the contact of torso with components of the

Table 2 Basic model parameter values

		Head	Torso
M_D	kg	15	45
k_{u1}^*	kN/m	0.3	0.3
d_{u1}^*	kNs/m	0.2	0.2
k_{v1}^*	kN/m	5.0	5.0
d_{v1}^*	kNs/m	1.7	10.0
k_{v2}^*	kN/m	175.0	700.0
d_{v2}^*	kNs/m	0.0	0.0
w_D	m	0.1	0.25
Δv	m	0.25	0.1

*Value averaged for the initial fragment of the characteristic curve

vehicle body structure and Fig. 14b shows the time history of the resultant acceleration of dummy's head. The dashed and solid lines in the graphs represent results of experimental tests and model simulations, respectively. For the motorcar collision, the effects of which have been presented as an example in Figs. 12 and 13, the injury arising process, that is simultaneously the dynamic deformation development process, is analysed till the instant $t = 0.06$ s from the beginning of the collision contact. Such interactions result in dynamic loads on the dummy, which can be observed with some delay due to the inertia of solid D and clearance Δv (Fig. 10). For this reason, the loads on the dummy were analysed till the instant $t = 0.1$ s.

For the calculation of the forecasted risk of impact-caused injuries, the factors of decisive importance are the extreme values of the loads observed [rib deflection, head acceleration, cf. (18) and (20)]. Within this

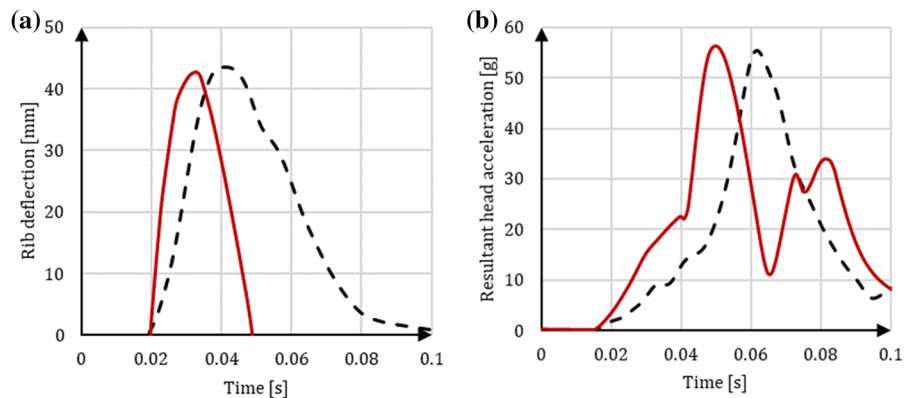


Fig. 14 Rib deflection (a) and resultant acceleration of dummy's head (b) in experimental tests (dashed line) and model calculations (solid line) for the side impact energy of 110 kJ

scope, the results of experimental tests and model simulations are consistent with each other. Table 3 shows a summary of the determined values of biodynamic indicators of head and torso injuries and the AIS 3+ injury probability values calculated on these grounds [Eqs. (21) and (22)].

2.4 Plan and scope of model tests

For model calculations, the model of a front-to-side motorcar collision and a dummy placed on driver's seat was used, which was prepared in accordance with the schematic diagram shown in Fig. 3 and with the description provided in Sects. 2.1–2.3. In the calculations, the impact energy values of the range 30–350 kJ, vehicle speed values of 30–60 km/h, and impacted vehicle's mass of 1000–3500 kg were taken into account. The impact energy range as specified above covers the cases ranging from an impact of a medium-class passenger car moving with a speed of 30 km/h (the impact energy of 30 kJ) to an impact of a passenger car or delivery vehicle with a gross vehicle mass of 3500 kg moving with a speed of 60 km/h (the impact energy of 350 kJ). The calculations were carried out for accidents taking place on a road with a dry asphalt-concrete surface. An assumption was also

made that the impacted vehicle was not moving immediately before the collision.

The calculations showing the connection between the probability of injury and the side impact energy were based on the values of biodynamic indicators of injuries to the head and torso of a dummy placed on driver's seat. For the research scope as specified above, the share of the energy of deformation of the vehicle body side zones in the process of energy dissipation during the collision was also determined.

3 Computation results and analysis thereof

To calculate individual components of the energy balance, the methods described in Sect. 2 were taken as a basis. The work of deformation of the s th zone of vehicle B body (Fig. 6) at the instant t_j was calculated from the equation:

$$W_{DBs}(t_j) = W_{DBs}(t_{j-1}) + 0.5 \cdot [R_{Bsn}(t_j) + R_{Bsn}(t_{j-1})] \cdot [c_{Bs}(t_j) - c_{Bs}(t_{j-1})], \quad (23)$$

where c_{Bs} —depth of deformation of the s th zone of vehicle B body. Its determined from the equation:

Table 3 Summary of example values of the injury indicator and risk after the validation

Side impact energy = 110 kJ	HIC36	Head Injury Risk AIS 3+	Max rib deflection [mm]	Torso Injury Risk AIS 3+
Model calculations	268	0.005	41.7	0.594
Experimental tests	281	0.006	42.0	0.599

$$c_{Bs}(t_j) = p_{Bs}(t_j)/b_s, \tag{24}$$

where: b_s —width of the zone B_s (Fig. 7); $p_{Bs}(t_j)$ —deformation area of zone B_s limited by the edges of the zone and boundary deformation line (Fig. 6).

The change in the kinetic energy of vehicle B is determined from the equation:

$$E_{KB}^*(t_j) = 0.5 \cdot M_B \cdot v_B^2(t_j) + 0.5 \cdot J_{CB} \cdot \dot{\psi}_B^2(t_j) - E_{KB}, \tag{25}$$

where $v_B = \sqrt{x_{0B}^2 + y_{0B}^2}$ —resultant linear velocity of vehicle B body, determined on the grounds of the first derivative of generalised coordinates [cf. (3)].

Figure 15 shows time histories of the growth in deformation depth c_{Bs} and force R_{Bsn} for several zones of the vehicle side. This result has been shown using as an example a front-to-side collision where the side impact energy is $E_{SI} = 72$ kJ. In this example, vehicle A with a mass of $M_A = 1532$ kg struck vehicle B with a speed of $v_A = 48$ km/h and the compression phase is considered whose end (time t_{END}) has been assumed as the instant of the maximum dynamic deformation of vehicle bodies. For this collision phase, the risk of injury to vehicle occupants has been calculated.

Based on the curves in Fig. 15, the deformation work was calculated for individual zones of vehicle B body, according to Eq. (23). The calculation results have been shown in Fig. 16. They represent time histories of changes in the deformation work values (W_{DBs}) for individual zones and in the percentage shares of W_{DBs} in the total work of deformation of the vehicle body side. The total deformation work was calculated for the end of the compression phase $W_{DB}(t = t_{END})$:

$$W_{DB}(t = t_{END}) = \sum_{s=1}^7 W_{DBs}(t = t_{END}). \tag{26}$$

The results obtained show that a significant part of the side impact energy is consumed by the deformation of the area of driver’s door (zone $B3$). This exceeds the work of deformation of pillar B (zone $B4$) by 15%. The model under consideration also shows the differences between the energy absorption of the rear and front door of the vehicle under test. This model used to analyse a front-to-side collision with an impact energy of 72 kJ shows that merely 18 kJ and 9.5 kJ of that energy is consumed by the deformation of the front and rear door, respectively, where both of these structural components are within the collision contact area in question (Fig. 7).

Tests were carried out with various values of the impact energy of vehicle A. The nonlinear elastoplastic and damping characteristics of individual vehicle body zones have exposed the variations in the proportions between the energy absorbed within the said zones and the side impact energy. The computation results have been presented in Fig. 17b in the form of relations between the values of these components and the side impact energy. In Fig. 17a, the values of the energy balance components have been shown as their percentage ratios to the side impact energy, which was calculated according to (2).

The calculation results shown in Fig. 17a confirm the nonlinear nature of dissipation of the front-to-side collision energy. In the front-to-side collision, the deformation of the front part of the impacting vehicle’s body is smaller than the deformation of the impacted vehicle’s body side. The properties of the vehicle body front are approximately linear within the

Fig. 15 Deformation depth (a) and force (b) for several zones of the vehicle B side during the compression phase

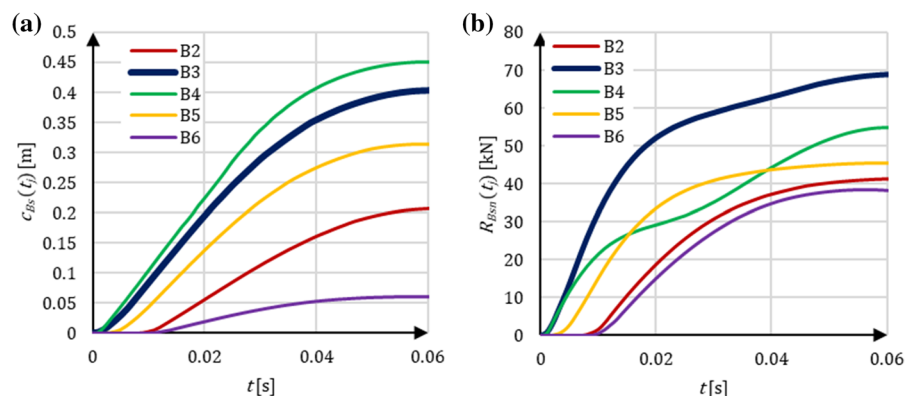


Fig. 16 Work of deformation of zones B2–B6 of the vehicle body side (a) and its percentage share in the total deformation work (b)

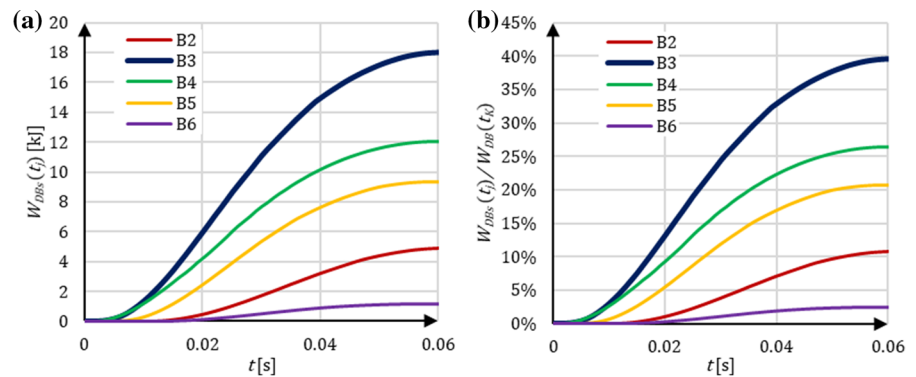
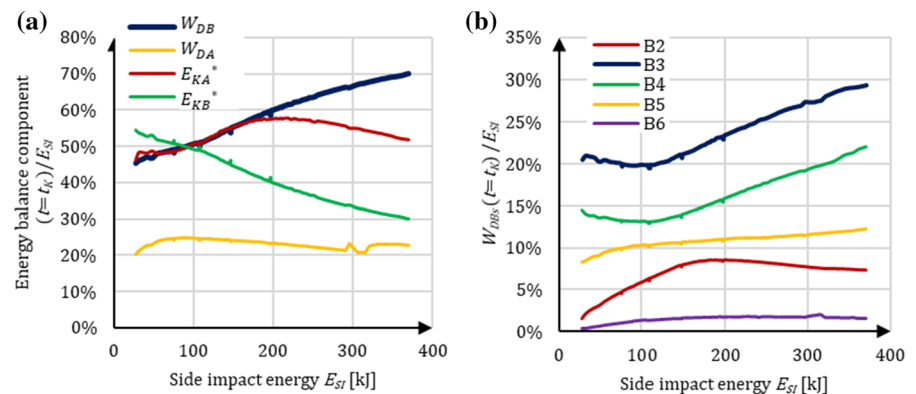


Fig. 17 Percentage shares of individual components of the collision energy balance (a) and of the work of deformation of individual zones of the vehicle body side (b) vs the side impact energy for $t = t_{\text{END}}$



deformation range in question. This manifests itself (the W_{DA} curve in Fig. 17a) in almost constant share of the vehicle A body deformation work in the side impact energy. However, the bigger side impact energy, the lower percentage share of the kinetic energy received during the collision by vehicle B (the E_{KB}^* curve in Fig. 17a). This takes place simultaneously with a growth in the share of vehicle B body deformation work in the side impact energy (the W_{DB} curve in Fig. 17a). For $E_{SI} < 90$ kJ, we have $E_{KB}^* > W_{DB}$, which shows that the growth in the kinetic energy of vehicle B makes a predominating part of the side impact energy. For this range of the impact energy, therefore, the risk of injury to the vehicle driver will be related to a greater extent to the inertial loads (lateral acceleration of the impacted vehicle's body) than to the process of deformation of the vehicle body side. In spite of the fact that for high values of the side impact energy, the change in the kinetic energy of the impacted vehicle makes only 30–40% of the impact energy, this change constitutes a source of a significant injury risk. The computation results presented in Fig. 17a indicate as well that the

model developed will be useful for improving the design of the vehicle body side structure.

The pointing out of the share of the vehicle body side deformation work W_{DB} as a function of the side impact energy highlights the process of an increase in the hazard to vehicle occupants. Simultaneously, the research conducted this way has made it possible to determine the relationship between the hazard to vehicle occupants and the values of biomechanical indicators (Fig. 14). This was used for the forecasting of the risk of injury to the head and torso of the driver of the impacted vehicle B. The injury risk was defined according to the AIS (Abbreviate Injury Scale) code. The example injury risk defined as AIS 3+ was estimated on the grounds of Eqs. (21) and (22). The injury risk was computed for vehicle occupant's torso at the AIS 3+ and AIS 4+ levels and for occupant's head at the AIS 2+, AIS 3+, and AIS 4+ levels. The computation results have been shown as functions of the side impact energy in Figs. 18 and 19, where the injury risk was indicated by red marks. At the same time, the results of the front-to-side impact crash tests carried out by NHTSA [12] were analysed. For the

Fig. 18 Risk of the AIS 3+ (a) and AIS 4+ (b) torso injury vs the side impact energy (for details see the text)

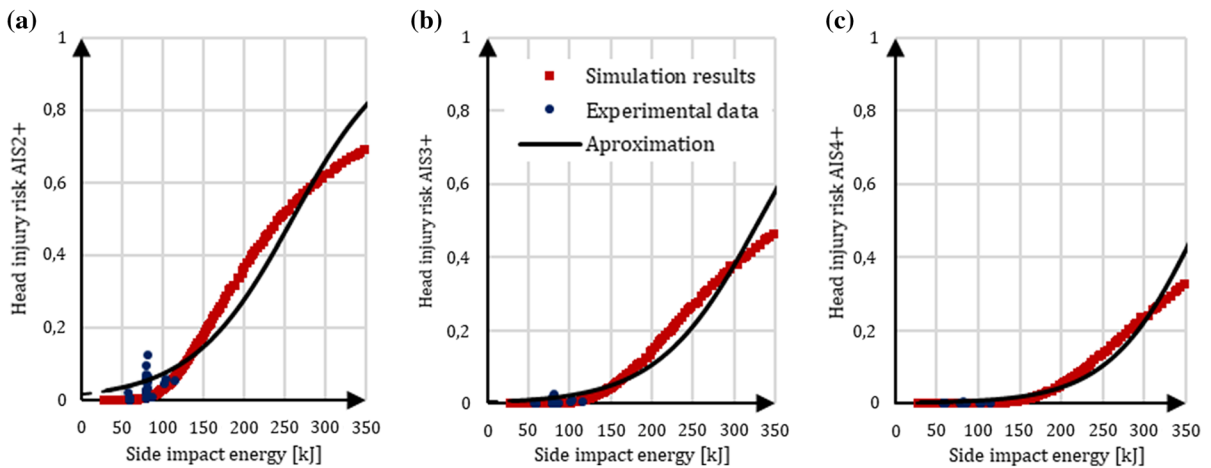
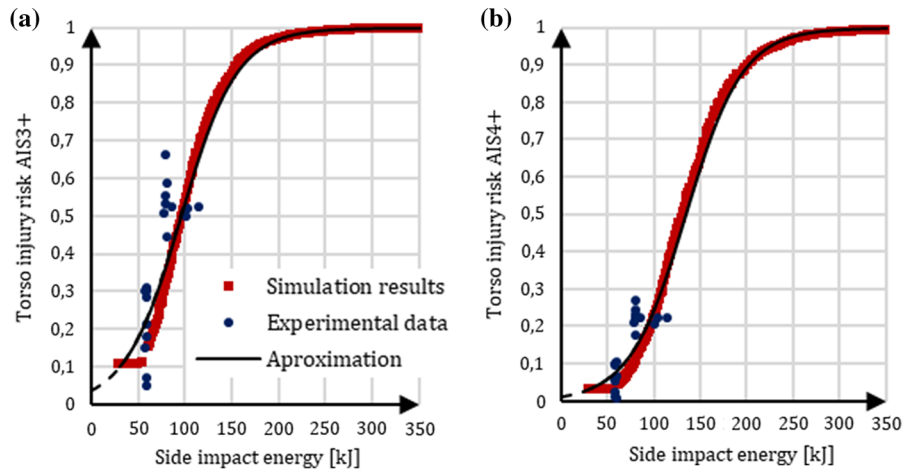


Fig. 19 Risk of the AIS 2+ (a), AIS 3+ (b), and AIS 4+ (c) head injury vs the side impact energy (for details see the text)

analysis, the experimental test results were selected that were obtained for cars with sedan-type bodies, of the class and year of manufacture being close to those assumed in the model tests. The group of experimental tests chosen for the analysis was the same as that whose results were used in the model validation process.

Based on results of those tests, the head and torso injury risks depending on the side impact energy were calculated and considered as experimental test results; these results are given in Figs. 18 and 19 and indicated by dark marks. Thus, two sets of test results have been presented in these graphs: model test results marked in red and experimental test results marked in a dark colour. The test results were approximated using the logit model [48–50], which is very often employed to

analyse the road traffic safety issues. The model was adopted in the form:

$$\text{Injury Risk} = \frac{e^{a+b \cdot E_{SI}}}{1 + e^{a+b \cdot E_{SI}}}, \quad (27)$$

where a and b are model coefficients calculated by the regression method and E_{SI} is the side impact energy expressed in [kJ].

For the computations, the environment of the Statistica programme [51] was used. The model coefficients were approximated for the E_{SI} values in the interval from 30 to 350 kJ. The a and b coefficient values for the head and torso injury risk functions have been gathered in Table 4; the curves representing these functions, plotted for several AIS injury severity

Table 4 Coefficients a and b of the regression function of the torso and head injury risks

	Injury scale	a	b
Torso	AIS 3+	− 3.369	0.017
	AIS 4+	− 4.731	0.018
Head	AIS 2+	− 5.008	0.011
	AIS 3+	− 6.458	0.013
	AIS 4+	− 8.215	0.013

levels, have been shown in Figs. 18 and 19 as black lines.

The research results presented in Figs. 18 and 19 show the relation between the energy of a side impact of a passenger car with a sedan-type body and the risk of injury to driver's head and torso. The side impact energy defined herein constitutes a predicate of the risk of injury to the vehicle driver. The research results indicate that the injury risk is much higher for the torso than that for the head at the same energy of the side vehicle impact. This is confirmed when the results of experimental tests [12] are compared with the results of model computations. The regression functions having been prepared make it possible to calculate the injury risk based on the side impact energy. In turn, an inverse procedure, i.e. determining the side impact energy based on a description of the injury to the vehicle driver, may be an important stage in the actions taken within the road accident reconstruction process, where the goal is to determine the state of pre-collision motion of the vehicles involved.

4 Discussion

The research being carried out offers the possibility of getting to know the relation: road accident—impact energy—risk of injury to vehicle occupants. In this study, the following relation predominates within this scope: road accident—forces acting during the collision—biomechanical injury indicators—injury risk [49, 52]. At present, additional relations are sought in terms of the relation: road accident—crash tests—impact energy. The results obtained from such explorations provide knowledge about the course of the nonlinear energy-related processes that take place during the compression phase of a front-to-side

collision of motor vehicles. The energy balance for the collision of this type has been determined in [34]. It has been determined that the energy dissipated for the deformation of the sedan car bodies makes 30–36% of the initial energy (collision energy). A comparison of results of such calculations with results of computer simulations carried out within this work has been presented as an example in Fig. 12b. The nature of the course of changes in the values of individual components of the energy balance is consistent for both publications, if the same values of the side impact energy are considered.

The values of the characteristic components of the energy balance in the experimental and model tests have been compared in Table 5. Good conformity was obtained for the work of deformation of the bodies of vehicles A and B, i.e. $W_{DAB}(t = t_{END})$. The change in the kinetic energy of vehicle B in result of the side impact, i.e. $E_{KB}^*(t = t_{END})$, calculated for the model, was somewhat smaller than that determined experimentally.

The conformity between the values calculated in model tests and determined experimentally, obtained in a few comparisons (shown above), enables the use of model test results for the analysis of some processes taking place during a road accident. Another comparison concerns [22], where results of computations of the injury risk expressed as a function of the Delta-V predicate have been presented. For a front-to-side collision where Delta-V is 32–40 km/h, the total risk of an AIS 4+ injury was estimated at 5–13%. To compare the results of that research with the results obtained within this work, come additional calculations were carried out:

- For the vehicle B mass of 1500 kg, the kinetic energy $E_{KB}^*(t = t_{END})$ corresponding to a change in the vehicle speed by 32 km/h and by 40 km/h was calculated.
- Using the data shown in Fig. 17, the value of $W_{DB}(t = t_{END})$ corresponding to the said energy was determined.
- The E_{SI} value was calculated, based on Eq. (2), and then the risk of head and torso injury forecast (Table 4 and Figs. 18 and 19).

The total injury risk P_{Joint} in [22] was calculated from indicators:

Table 5 Energy balance component values determined in the experimental and model tests

	Results of experimental tests [23]	Numerical simulations carried out within this work
E_{SI} [kJ]	72	
$W_{DAB}(t = t_{END})$ [kJ]	73	72
$E_{KB}^*(t = t_{END})$ [kJ]	55	46

$$P_{\text{Joint}} = [1 - (1 - P_{\text{Head}}) \cdot (1 - P_{\text{Torso}})] \cdot 100\%, \quad (28)$$

where: P_{Head} , P_{Torso} —head and torso injury risk, respectively.

As a result, the total injury risk value at a level of 1–10% was obtained, which is close to the results given in [22]. The results of these actions have been gathered in Table 6.

The relation between the AIS 3+ and AIS 4+ injury and the speed of a side impact against a concrete barrier was determined in [28]. The special course of a collision of this type (impact against a rigid undeformable barrier) makes it possible to assume that the side impact energy is approximately equal to the vehicle's kinetic energy at the instant of the impact. For a side impact speed of 36 km/h, the risk of AIS 3+ and AIS 4+ torso injury was determined as about 91% and 80%, respectively [28]. Assuming the vehicle mass as 1 500 kg, the side impact energy for such a speed is 75 kJ. According to the results obtained now (during the analysis of the front-to-side vehicles' collision), the torso injury risk for $E_{SI} = 75$ kJ would be 33% (AIS 3+) and 13% (AIS 4+).

The calculations like these show the influence of the energy absorption by the vehicle side being deformed and of the energy dissipation on the sliding of vehicle B during the impact. Due to disregarding the energy absorption and dissipation factors mentioned above, the injury risk was estimated in [28] at 80–91%. However, if these factors are taken into account

(during vehicles' collision) then the value of this risk drops to 13–33%, according to the present calculations.

The calculation results obtained, supplemented with experimental test results, indicate the usefulness of the method of analysing the relation: road accident—crash tests—vehicle impact energy—risk of injury to vehicle occupants, as used herein. The approach to the analysis of the injury risk based on the course of energy-related processes, as adopted in this work, has proved to be a reasonable method suitable for the analysis of front-to-side collisions. Such collisions are more complicated than the well-explored frontal collisions. The problems with using the Delta-V predicates for analysing the road accident effects in frontal and side collisions have been highlighted e.g. in [31]. The energy balance analysis of the process where an injury risk arises during a road accident is an approach more universal than the use of a predicate related to the change in vehicle speed in result of a collision. In this work, a predicate in the form of the side impact energy has been proposed. Since good conformity was obtained between the results of experimental and model tests as regards the relations between the values of this predicate and the injury risk (Figs. 18 and 19), a conclusion may be drawn that the nature of the relation thus determined between the course and effects of a road accident is correct.

Table 6 Injury risk calculation results

Impact speed [km/h]	32	40
Injury risk calculated in [21]	5%	13%
$E_{KB}^*(t = t_{END})$ [kJ]	60	90
$W_{DB}(t = t_{END})$ [kJ]	67	156
E_{SI} [kJ]	127	246
AIS 4+ injury risk calculated now according to (27)	1%	10%

5 Summary and conclusions

When the relations were sought in this work between the energy of a side impact against a motor vehicle and the risk of injury to the vehicle occupants, the experimental test results available and the models specially built for this purpose in the MATLAB programme were used. The experimental test results were taken as a basis to validate the model of a collision-caused deformation of a vehicle body side, to evaluate the impact of the vehicle body side being deformed on the dummy driver, and to determine the kinematics of the impacted vehicle in its post-collision motion. Similarly, the final calculation results, i.e. the injury risk characteristics, were referred to crash test results and were found to be quite close to each other. The comparisons of this kind between the results of model calculations and crash test results have been presented in Fig. 12b from the energy balance point of view and in Figs. 18 and 19 in terms of injury risk.

The research carried out has confirmed the reasonability of using the injury risk characteristics considered as functions of the side impact energy. In result of that, a computational relation (the logit model) between the side impact energy and the risk of injury according to the Abbreviated Injury Scale has been determined. Thanks to the energy-related approach adopted for the processes that take place during the front-to-side vehicle collision, the following findings could be formulated:

- The process of dissipation of the front-to-side collision energy is nonlinear and the work of deformation of the front part of the impacting vehicle's body is much smaller than the work of deformation of the impacted vehicle's body side, regardless of the impact energy value (Fig. 17a).
- The risk of injury to the driver/occupant of the vehicle struck on its side arises from a change in the kinetic energy of the impacted vehicle (usually this is a momentary growth in its energy) and from an excessive penetration of the vehicle body side into the passenger compartment of the car.
- The diversified shares of the energy of deformation of individual zones on a car body side (Fig. 7) in the energy dissipation process during the side impact (Fig. 17b) provide a reasonable basis for improving the design of the vehicle body side structure.
- The use of a new predicate for analysing the front-to-side vehicle collision has been substantiated. In particular, the characteristics formulated by using this predicate have an important feature: the side impact energy can be easily determined from the vehicle side deformation and from the lateral slide of the vehicle during the collision. Additionally, the research carried out has provided grounds for the following conclusions:
 - During a side impact, the injury risk is much higher for the torso than that for the head regardless of the impact energy value (Figs. 18 and 19).
 - At the side impact energy value lower than 90 kJ, its predominating part causes a change in the kinetic energy of the impacted vehicle; hence, the risk of injury to vehicle occupants will mainly arise from the inertial forces' action on the occupants.
 - At impacts with the energy value exceeding 90 kJ, a predominating share of the work of deformation of the vehicle body side in the impact energy can be seen; therefore, the penetration of the vehicle body side into the passenger compartment of the car considerably increases the risk of injury to vehicle occupants (Fig. 17a).

The research carried out has provided grounds for confirming the fact that the course of a front-to-side vehicle collision in model simulations and in experimental tests is mutually consistent, in terms of energy balance (Fig. 7b). The calculation results obtained in the research reported herein are coherent with the results of front-to-side crash tests and the side impact energy has proven to be a good predicate of the effects of the road accidents under consideration. This provides grounds for further development of the research tool having been prepared, e.g. in the area of improving the passive safety of the motorcar body side.

Acknowledgements The authors acknowledge the Organizing Committee of the 16th International Conference "Dynamical Systems—Theory and Applications" (DSTA 2021) for received recommendation of this article.

Authors contributions Conceptualisation and methodology to the study were contributed by LP and MZ. Modelling, validation and calculations were performed by KD, MZ and PS. Results was prepared by MZ and PS. Formal analysis and investigation were carried out by LP and MZ. Original draft of the article was written by MZ. Review and final editing was performed by LP.

Project administration and funding acquisition was realised by MZ. All authors read and approved the final manuscript.

Funding This work was co-financed by Military University of Technology under research project UGB 22–882/2021.

Competing interests The authors have no relevant financial or non-financial interests to disclose.

Open Access This article is licensed under a Creative Commons Attribution 4.0 International License, which permits use, sharing, adaptation, distribution and reproduction in any medium or format, as long as you give appropriate credit to the original author(s) and the source, provide a link to the Creative Commons licence, and indicate if changes were made. The images or other third party material in this article are included in the article's Creative Commons licence, unless indicated otherwise in a credit line to the material. If material is not included in the article's Creative Commons licence and your intended use is not permitted by statutory regulation or exceeds the permitted use, you will need to obtain permission directly from the copyright holder. To view a copy of this licence, visit <http://creativecommons.org/licenses/by/4.0/>.

References

- Road traffic accidents in Poland in 2020. Polish Police Headquarters. Road Traffic Office, Warsaw (2020)
- Rattenbury, S.J., Gloyns, P.F., Nolan, J.M.: Vehicle deformation in real-world side impact crashes and regulatory crash tests (No. 2001*06-0248). SAE Technical Paper (2001)
- Ganesh, T.S., Bansode, P., Revankar, V., Kumar, S.: Vehicle performance evaluation in side impact (MDB) using ES-II dummy. In: IOP Conference Series: Materials Science and Engineering (vol. 314, no. 1, p. 012021). IOP Publishing, Bristol (2018, February) <https://doi.org/10.1088/1757-899X/314/1/012021>
- Arbelaez, R.A., Baker, B.C., Nolan, J.M.: Delta Vs for IIHS side impact crash tests and their relationship to real world crash severity. In: 19th ESV Conference, Paper (2005, June)
- National Highway Traffic Safety Administration, U.S. Department of Transportation, Federal Motor Vehicle Safety Standards No. 214, Side Impact Protection, Washington 2000
- McGwin, G., Jr., Modjarrad, K., Duma, S., Rue, L.W., III.: Association between upper extremity injuries and side airbag availability. *J. Trauma Acute Care Surg.* **64**(5), 1297–1301 (2008). <https://doi.org/10.1097/TA.0b013e3181271b21>
- Kirk, A., Morris, A.: Side airbag deployments in the UK-Initial case reviews. In 18th International Technical Conference on the Enhanced Safety of Vehicles. (2003, May)
- Bendjaballah, D., Bouchouha, A., Sahli, M.L., Gelin, J.C.: Numerical analysis of side airbags deployment in out-of-position situations. *Int. J. Mech. Mater. Eng.* **12**(1), 1–9 (2017). <https://doi.org/10.1186/s40712-016-0070-2>
- Summers, S.M., Prasad, A., Hollowell, W.T.: NHTSA's research program for vehicle aggressivity and fleet compatibility. In: National Highway Traffic Safety Administration, USA, Paper #249
- Gabler, H.C.: The evolution of side crash compatibility between cars, light trucks and vans. *SAE Int.* (2003). <https://doi.org/10.4271/2003-01-0899>
- Gabler, H.C., Hollowell, G.W.: The Aggressivity of Light Trucks and Vans in Traffic Crashes. SAE Technical Paper Series, Airbag Technology, SP-1333 <http://www.jstor.org/stable/44741082>
- National Highway Traffic Safety Administration Vehicle Crash Test Database, <https://www.nhtsa.gov/research-data/databases-and-software> (tests no 3799, 4097, 4380, 4455, 4456, 4562, 4609, 4862, 4902, 4934, 4941, 4981, 5044, 5046, 5048, 5146, 5151, 5156, 5157, 5161, 5244, 5256, 5260, 5376, 5377, 5386, 5396, 5451, 5475, 5476, 5477, 5482, 5483, 5575, 5747, 5885)
- Kelley, M.E., Talton, J.W., Weaver, A.A., Usoro, A.O., Barnard, E.R., Miller, A.N.: Associations between upper extremity injury patterns in side impact motor vehicle collisions with occupant and crash characteristics. *Accid. Anal. Prev.* **122**, 1–7 (2019). <https://doi.org/10.1016/j.aap.2018.09.029>
- Huh, H., Lim, J.H., Song, J.H., Lee, K.S., Lee, Y.W., Han, S.S.: Crashworthiness assessment of side impact of an auto-body with 60TRIP steel for side members. *Int. J. Automot. Technol.* **4**(3), 149–156 (2003)
- Teng, T.L., Chang, K.C., Nguyen, T.H.: Crashworthiness evaluation of side-door beam of vehicle. *Tech. Mech.* **28**(3–4), 268–278 (2008)
- Long, C.R., Yuen, S.T.E.E.V.E., Nurick, G.N.: Analysis of a car door subjected to side pole impact. *Latin Am. J. Solids Struct.* (2019). <https://doi.org/10.1590/1679-78255753>
- Njuguna, J.: The application of energy-absorbing structures on side impact protection systems. *Int. J. Comput. Appl. Technol.* **40**(4), 280–287 (2011). <https://doi.org/10.1504/IJCAT.2011.041657>
- Tay, Y.Y., Lim, C.S., Lankarani, H.M.: A finite element analysis of high-energy absorption cellular materials in enhancing passive safety of road vehicles in side-impact accidents. *Int. J. Crashworthiness* **19**(3), 288–300 (2014). <https://doi.org/10.1080/13588265.2014.893789>
- Ike, A.E., Owunna, I.B., Satope, P.: Design optimization of a B-pillar for crashworthiness of vehicle side impact. *J. Mech. Eng. Sci.* **11**(2), 2693–2710 (2017). <https://doi.org/10.15282/jmes.11.2.2017.11.0245>
- Marklund, P.O., Nilsson, L.: Optimization of a car body component subjected to side impact. *Struct. Multidiscipl. Optim.* **21**(5), 383–392 (2001). <https://doi.org/10.1007/s001580100117>
- MacKenzie, E.J., Shapiro, S., Eastham, J.N.: The Abbreviated Injury Scale and Injury Severity Score: levels of inter- and intrarater reliability. *Med. Care* **23**, 823–835 (1985)
- Viano, D.C., Parenteau, C.S.: Severe injury to near-and far-seated occupants in side impacts by crash severity and belt use. *Traffic Inj. Prev.* **11**(1), 69–78 (2010)
- Huang, M.: Vehicle crash mechanics. CRC Press, Boca Raton (2002)
- Vangi, D.: Vehicle collision dynamics: analysis and reconstruction. Butterworth-Heinemann, Oxford (2020)
- Pawlus, W., Karimi, H.R., Robbersmyr, K.G.: Investigation of vehicle crash modeling techniques. *Int. J. Adv. Manuf.*

- Technol. **70**, 965–993 (2014). <https://doi.org/10.1007/s00170-013-5320-3>
26. Lin, C.H.: Modeling and simulation of van for side impact sensing tests. In 20th Enhanced Safety Vehicles Conference, Lyon, France, June 18–22 (2007).
 27. Sousa, L., Verissimo, P., Ambrósio, J.: Development of generic multibody road vehicle models for crashworthiness. *Multibody Sys.Dyn.* **19**(1), 133–158 (2008). <https://doi.org/10.1007/s11044-007-9093-z>
 28. Tan, T.C., Grzebieta, R.H., McIntosh, A.S.: Review of flail-space's lateral impact velocity criterion for thoracic impacts. *J. Transp. Saf. Secur.* **9**(2), 239–258 (2017). <https://doi.org/10.1080/19439962.2016.1181690>
 29. Radu, A.I., Toganel, G.R., Trusca, D.D.: Mathematical model validated by a crash test to be used as kinematic and dynamic study for side impacts. *Int. J. Automot. Technol.* **22**(5), 1267–1277 (2021). <https://doi.org/10.1007/s12239-021-01111-6>
 30. Bareiss, M., Gabler, H.C.: Estimating near side crash injury risk in best performing passenger vehicles in the United States. *Accid. Anal. Prev.* **138**, 105434 (2020). <https://doi.org/10.1016/j.aap.2020.105434>
 31. Ji, A., Levinson, D.: An energy loss-based vehicular injury severity model. *Accid. Anal. Prev.* **146**, 105730 (2020). <https://doi.org/10.1016/j.aap.2020.105730>
 32. Lai, X., Ma, C., Hu, J., Zhou, Q.: Impact direction effect on serious-to-fatal injuries among drivers in near-side collisions according to impact location: focus on thoracic injuries. *Accid. Anal. Prev.* **48**, 442–450 (2012). <https://doi.org/10.1016/j.aap.2012.02.023>
 33. Prochowski, L., Ziubiński, M., Dziewiecki, K., Szwa-jkowski, P.: Impact energy versus the hazards for the occupants during a front-to-side vehicles' collision. In: 16th Conference on Dynamical Systems Theory and Applications DSTA 2021 Abstracts, Łódź, Poland, December 6–9 2021, pp. 473–474 (2021) <https://doi.org/10.34658/9788366741201>
 34. Gidlewski, M., Prochowski, L., Jemioł, L., Żardecki, D.: The process of front-to-side collision of motor vehicles in terms of energy balance. *Nonlinear Dyn.* **97**(3), 1877–1893 (2019). <https://doi.org/10.1007/s11071-018-4688-x>
 35. Prochowski, L., Ziubiński, M., Pusty, T.: Experimental and analytic determining of the characteristics of deformation and side stiffness of a motor car body based on results of side-impact crash tests. In: IOP Conference series: materials science and engineering (vol. 421, no. 3, p. 032025). IOP Publishing. (2018, September) <https://doi.org/10.1088/1757-899X/421/3/032025>
 36. Luty, W.: Tire transient properties in simulation of vehicle lateral dynamics in curvilinear motion, *Prace Naukowe Politechniki Warszawskiej. Transport. Oficyna Wydawnicza Politech. Warsz.* **98**, 357–367 (2013)
 37. Rill, G. TMeasy—a handling tire model based on a three-dimensional slip approach. In Proceedings of the XXIII International Symposium on Dynamic of Vehicles on Roads and on Tracks (IAVSD 2013), Qingdao, China, 19–23 August 2013
 38. Horiuchi, S., Okada, K., Nohtomi, S.: Numerical analysis of optimal vehicle trajectories for emergency obstacle avoidance. *JSAE Rev.* **22**(4), 495–502 (2001)
 39. Prochowski, L., Gidlewski, M., Ziubiński, M., Dziewiecki, K.: Kinematics of the motorcar body side deformation process during front-to-side vehicle collision and the emergence of a hazard to car occupants. *Meccanica* **56**(4), 901–922 (2021). <https://doi.org/10.1007/s11012-020-01274-3>
 40. Hirschberg, W., Rill, G., Weinfurter, H.: Tire model TMeasy. *Veh. Syst. Dyn.* **45**, 101–119 (2007). <https://doi.org/10.1080/00423110701776284>
 41. Zhao, P., Liu, J., Li, Y., Wu, C.: A spring-damping contact force model considering normal friction for impact analysis. *Nonlinear Dyn.* **105**(2), 1437–1457 (2021). <https://doi.org/10.1007/s11071-021-06660-4>
 42. Rong, B., Rui, X., Tao, L., Wang, G.: Theoretical modeling and numerical solution methods for flexible multibody system dynamics. *Nonlinear Dyn.* **98**(2), 1519–1553 (2019). <https://doi.org/10.1007/s11071-019-05191-3>
 43. Corral, E., Moreno, R.G., García, M.G., Castejón, C.: Nonlinear phenomena of contact in multibody systems dynamics: a review. *Nonlinear Dyn.* **104**(2), 1269–1295 (2021). <https://doi.org/10.1007/s11071-021-06344-z>
 44. Euro NCAP, <http://www.euroncap.com>
 45. Zhou, D., Wang, X., Zheng, Q., Fu, T., Wu, M., Sun, X.: A nonlinear occupant-restraint system model for predicting human injuries caused by vertical impact. *Nonlinear Dyn.* **105**(4), 3093–3115 (2021). <https://doi.org/10.1007/s11071-021-06490-4>
 46. Zaroni, A., Cocco, A., Masarati, P.: Multibody dynamics analysis of the human upper body for rotorcraft–pilot interaction. *Nonlinear Dyn.* **102**(3), 1517–1539 (2020). <https://doi.org/10.1007/s11071-020-06005-7>
 47. Kuppa, S.: Injury criteria for side impact dummies. National Transportation Biomechanics Research Center, NHTSA (2004)
 48. White, M.J.: The “arms race” on American roads: the effect of sport utility vehicles and pickup trucks on traffic safety. *J. Law Econ.* **47**(2), 333–355 (2004). <https://doi.org/10.1086/422979>
 49. Richards, D.C.: Relationship between Speed and Risk of Fatal Injury: Pedestrians and Car Occupants. Department of Transport, London (2010)
 50. Liu, S., Li, Y., Fan, W.D.: Mixed logit model based diagnostic analysis of bicycle-vehicle crashes at daytime and nighttime. *Int. J. Transp. Sci. Technol.* (2021). <https://doi.org/10.1016/j.ijst.2021.10.001>
 51. Statistica, StatSoft EUROPE, <https://www.statistica.com/en/>
 52. Bois, P.D., Chou, C.C., Fileta, B.B., Khalil, T.B., King, A.I., Mahmood, H.F., Mertz, H.J., Wismans, J., Prasad, P., Belwafa, J.E.: Vehicle Crashworthiness and Occupant Protection. American Iron and Steel Institute (2004)

Publisher's Note Springer Nature remains neutral with regard to jurisdictional claims in published maps and institutional affiliations.